Comparative Analysis of Epstein-Barr Virus EBNA-2 Sequence Variation in Nasopharyngeal Carcinoma and Other EBV-Related Tumors

Lee Wei Zheng[1,2], Rabiatul Basria S. M. N. Mydin[1*], Adam Azlan[1,5] , Muhamad Yusri Musa[3,4]

Abstract

Epstein Barr virus (EBV) is a common gamma herpesvirus that has infected over 95% of the worldwide population and is associated with several diseases which includes Hodgkin lymphoma (HL), Burkitt's lymphoma (BL), nasopharyngeal carcinoma (NPC) and gastric cancer (GC). Epstein Barr virus nuclear antigen 2 (EBNA-2) gene of EBV is pivotal for growth transformation process and EBV type differentiation. Variations of the EBNA-2 gene could affect EBV transformation. Thus, understanding the variations that occur could provide invaluable insights. Variations of the EBNA-2 gene of EBV from different countries and disease associated was identified by comparing the gene with the reference sequence of EBNA2 from EBV isolated from C666-1 with the accession KC617875. Out of 11 samples, KC440851 is the most diverged and distally related sample from the reference sample. Interestingly some disease share similarities within the EBNA-2 gene as in the case of BL and NPC. The divergence of ENBA-2 gene increases with respect to geographical region when compared to reference sample.

Keywords: cancer, disease, Epstein Barr virus (EBV), Epstein Barr virus nuclear antigen 2 (EBNA-2), variation

Significance | A study of virus related cancer

*Correspondence: Ts. Dr. Rabiatul Basria S. M. N. Mydin, Department of Biomedical Sciences, Advanced Medical and Dental Institute, Universiti Sains Malaysia, 13200 Kepala Batas, Pulau Pinang, Malaysia, E-mail: rabiatulbasria@usm.my

Editor Mohammad Russel And accepted by the Editorial Board Nov 12 2023 (received for review Sep 28, 2023)

Introduction

Epstein Barr virus (EBV) also known as human herpesvirus 4 (HHV-4) is a ubiquitous and oncogenic gammaherpesvirus that has infected over 95% of the worldwide population ranging from asymptomatic to infectious mononucleosis (Womack & Jimenez, 2015). EBV is implicated in the pathogenesis of Hodgkin lymphoma, nasopharyngeal carcinoma, gastric cancer, and numerous malignancies in individuals with inherited or acquired immunodeficiency (Matthew & Razelle, 2004). EBV infects B cells and resides in memory B cells in healthy people to establish a life-long persistence in the human host in asymptomatic individuals and does not cause disease. EBV persistently infects memory B-cells due to the prevalence of the CD21 receptor present on the surface of B-cells (Sugano et al., 1997). CD21 receptor acts as the major cellular receptor for EBV as CD21 interacts with the EBV glycoprotein (Busse et al., 2010). Epstein Barr virus nuclear antigen 2 (EBNA-2) is a gene encoded by EBV that is essential for the growth transformation process and a major determinant of the differences between EBV-1 and EBV-2 subtype in lymphocyte growth transformation (Cohen et al., 1989).

In this study, the EBV EBNA2 gene that was used as reference samples is from the C666-1 cell line, an undifferentiated nasopharyngeal carcinoma (NPC) from a subclone of its parental cell line, C666, derived from an NPC xenograft of southern Chinese origin where the GenBank accession number is KC617875 (Cheung et al., 1999). This cell line consistently

Author Affiliation:
[1]Department of Biomedical Sciences, Advance Medical and Dental Institute, Universiti Sains Malaysia, 13200 Kepala Batas, Pulau Pinang, Malaysia.
[2]School of Biological Sciences, Universiti Sains Malaysia, 11800 Gelugor, Pulau Pinang, Malaysia
[3]Pusat Perubatan USM Bertam, Universiti Sains Malaysia, 13200 Kepala Batas, Pulau Pinang, Malaysia.
[4]Department of Clinical Medicine, Advance Medical and Dental Institute, 13200 Kepala Batas, Pulau Pinang, Malaysia.
[5]School of General and Foundation Studies, Asian Institute of Medicine, Science and Technology (AIMST University), 08100, Bedong, Kedah, Malaysia.

Please cite this article:
Lee Wei Zheng, Rabiatul Basria S. M. N. Mydin, Adam Azlan, Muhamad Yusri Musa, (2023), Comparative Analysis of Epstein-Barr Virus EBNA-2 Sequence Variation in Nasopharyngeal Carcinoma and Other EBV-Related Tumors, Journal of Angiotherapy, 7(1), 1-9, 9352

maintains EBV in long-term culture, providing an excellent in vitro model for EBV and NPC studies (Cheung et al., 1999). Maximum likelihood is the technique used for this study in the estimation of evolutionary trees from nucleic acid sequence data which is not likely to give misleading results if rates of evolution differ in different lineages. In addition, it also allows testing of assumptions about evolutionary rate constancy via likelihood ratio tests and gives a rough indication of the error in tree estimates (Felsenstein, 1981). Studying the diversity of EBV EBNA2 in various disease is pivotal as this gene could act as a transcription factor in activating crucial downstream elements. Elucidating the differences of EBNA2 across diseases could provide valuable insights on its functioning.

Materials and Method

FASTA Sequence Searching

The FASTA sequences of the EBNA-2 region for Epstein-Barr virus (EBV) were found, retrieved, and downloaded from the National Center for Biotechnology Information (NCBI) database. The EBV FASTA sequences were identified for the country or region, type, disease-associated and isolate by using the NCBI accession code. The downloaded FASTA sequences were then combined into 1 sequence data file before being loaded.

Creating Multiple Sequence Alignments

An alignment was created from nucleotide sequence data that will be imported into the alignment editor. The Alignment Explorer was launched by selecting the Align | Edit/Build Alignment menu command. Create New Alignment was selected and Ok clicked. The button labelled DNA was clicked. To align sequences contained in a sequence data file, first, the unaligned sequences, which is the combined FASTA sequence data file are added into the Alignment Explorer by clicking selecting the Data | Open | Retrieve Sequences from the File menu command. Then, the Edit | Select All menu command was selected to select all sites for every sequence in the data set. Next, the Alignment | Align by ClustalW menu command was selected to align the selected sequences data using the ClustalW algorithm. The OK button was clicked to run ClustalW analysis at default settings. Lastly, the current alignment session was saved by selecting the Data | Save Session menu command.

Model Analysis and Phylogenetic Tree Construction

Once the sequence has been aligned, the Data | Phylogenetic Analyses icon on the tab is clicked. The aligned sequence was then analysed by clicking on Model | Find Best DNA/Protein Models (ML) to look for the best-fits nucleotide models with the maximum likelihood statistical method. Next, the model with the lowest BIC scores (Bayesian Information Criterion), which is the Hasegawa-Kishino-Yano with gamma-distributed and invariant sites model was selected to create a phylogenetic tree. Out of 3 types of phylogenetic trees, which are Maximum Likelihood, Neighbour-joining and Minimum evolution tree, Maximum Likelihood was used. The phylogenetic trees were constructed by using original and bootstrap data. To create phylogenetic trees, first, the Phylogeny | Construct/Test Maximum Likelihood Tree menu command was selected from the main MEGA window launch bar. The Analysis Preferences window will appear, and the test of phylogeny was set as none. Then, the nucleotide substitution type was clicked. Nucleotide was clicked for substitution type and the Hasegawa-Kishino-Yano model was selected. Next, the rate among sets was set at gamma distributed with invariant sites (G+I) and the number of discrete gamma categories was set at 5. The OK button was clicked to construct a phylogenetic tree. For the bootstrap phylogenetic tree, a test of phylogeny was set to bootstrap, and the bootstrap value was set to 100.

Result & Discussion

Gene accession number, phenotype, and country mined for 11 samples and 1 reference sample of Epstein-Barr virus with Epstein-Barr virus nuclear antigen 2 (EBNA-2) gene were retrieved from the NCBI database (table 1). EBNA-2 sequence from 4 diseases which includes Nasopharyngeal Carcinoma, Burkitt Lymphoma, gastric cancer, and Hodgkin Lymphoma were used. These samples are respectively from 6 different countries namely China, Japan, Kenya, South Korea, Poland, and the United Kingdom.

The accession number of 1 reference sample and 11 samples are listed in the first column. In the second listed the disease associated and the third column listed the country the the EBV is isolated.

Mutation sites of each EBV EBNA-2 gene according to the mutation type which are missense, silent, insertion, deletion and unknown mutation were identified and significant mutations except for silent mutation were categorised and shown in table 2.1 to 2.4 and Figure 1. Missense mutations are significant mutation that causes changes in the amino acid sequence, while silent mutation does not change or affect the amino acid sequence. Insertion and deletion of nucleotides may give rise to different results on amino acids. Lastly, there is also an unknown mutation identified.

Missense mutation

The nucleotide sites changed for each sample when compared with reference gene KC617875 are listed in the first column.

The accession number of samples that have the corresponding mutation is listed in the second column. In the third column, the amino acid changes that are caused by the missense nucleotide mutation are listed.

Table 1: List of EBV EBNA-2 genes from different phenotypes and countries.

Nucleotide Accession Number	Phenotype	Country
KC617875 (Reference gene)	NPC	China
MK540313	NPC	China
MK540314	NPC	China
MK540359	NPC	China
AY961628	NPC	China
MK540241	Burkitt Lymphoma	China
KC207813	Burkitt Lymphoma	Japan
KC207814	Burkitt Lymphoma	Kenya
MG021307	Gastric cancer	South Korea
MG021308	Gastric cancer	Poland
KC440851	Gastric cancer	United Kingdom
LN824204	Hodgkin Lymphoma	United Kingdom

Table 2.1: Missense mutation sites of each EBV EBNA-2 gene by comparing to reference sample (KC617875)

Nucleotide Change	Gene Accession Number	Amino Acid Change
C67G	AY961628, KC207813	R23V
G68A	MG021307	R23H
G68T	All except MG021307	R23L
C126A	LN824204	D42E
C185T	MK540241, MK540313, MK540314, MK540359	P62L
C238T	MG021308	P80S
Y247T	KC207814	?83P
Y247C	All except KC207814	?83S
C256T	KC207814, MG021308	P86S
Y265T	All except KC440851	?89S
Y265C	KC440851	?89P
A343T	AY961628	R115W
G453T	All except (MK540241, MK540313, MK540314, MK540359)	M151I
G487A	All except (KC207814 & MG021308)	V163M
T488G	MK540241, MK540313, MK540314, MK540359	V163R
G554A	AY961628, KC207813, KC440851, LN824204, MG021307	R185Q
C584T	All except (MK540241, MK540313, MK540314, MK540359)	T195M
G588T	KC207814 & MG021308	M196I
A610T	KC207814 & MG021308	T204S
G659A	MG021308	R220H
A737C	All except (MK540241, MK540313, MK540314, MK540359)	Q246P
A739C	All except (MK540241, MK540313, MK540314, MK540359)	S247R
A842C	All except (MK540241, MK540313, MK540314, MK540359)	N281T
C949A	KC207814 & MG021308	H317N
G1183A	KC440851	G395R
A1424T	KC207814, MK540313, MK540359	Y475F
G1430A	All except (KC207814 & MG021308)	G477E
T1456C	KC207814 & MG021308	S486P
C1460T	All except (MK540241, MK540313, MK540314, MK540359)	T487I

Table 2.2: Deletion mutation sites of each EBV EBNA-2 gene by comparing to reference sample (KC617875)

Nucleotide Change	EBV Type	Amino Acid Change
185_286del	AY961628	P62 ; 63_95del ; P96
198_203del	KC207814, MG021308	P66 ; 67del ; P68
200_202del	KC207813, MG021307	P67 ; P68
1072_1077del	AY961628	358_359del

Table 2.3: Insertion mutation sites of each EBV EBNA-2 gene by comparing to reference sample (KC617875)

Nucleotide Change	EBV Type	Amino Acid Change
633_637insCTC	KC207814 & MG021308	212insL

Table 2.4: Unknown mutation sites of each EBV EBNA-2 gene by comparing to reference sample (KC617875)

Nucleotide Change	EBV Type	Amino Acid Change
172_303	LN824204	58_101
1022_1081	LN824204	341_361

Table 3: Maximum likelihood fits of 24 different nucleotide substitution models

Model	Parameters	BIC	AICc	*lnL*	(+*I*)	(+*G*)	*R*	*f*(A)	*f*(T)	*f*(C)	*f*(G)	*r*(AT)	*r*(AC)	*r*(AG)	*r*(TA)	*r*(TC)	*r*(TG)	*r*(CA)	*r*(CT)	*r*(CG)	*r*(GA)	*r*(GT)	*r*(GC)
HKY+G+I	27	5067.382	4858.060	-2401.986	0.48	0.05	1.80	0.261	0.184	0.365	0.190	0.032	0.063	0.125	0.045	0.239	0.033	0.045	0.121	0.033	0.171	0.032	0.063
HKY+G	26	5067.551	4865.978	-2406.948	n/a	0.05	1.75	0.261	0.184	0.365	0.190	0.032	0.064	0.123	0.046	0.237	0.033	0.046	0.120	0.033	0.170	0.032	0.064
TN93+G	27	5075.247	4865.925	-2405.918	n/a	0.05	1.76	0.261	0.184	0.365	0.190	0.032	0.064	0.090	0.046	0.289	0.033	0.046	0.146	0.033	0.123	0.032	0.064
TN93+G+I	28	5075.460	4858.389	-2401.147	0.48	0.05	1.82	0.261	0.184	0.365	0.190	0.032	0.063	0.092	0.045	0.291	0.033	0.045	0.147	0.033	0.126	0.032	0.063
HKY+I	26	5087.133	4885.561	-2416.740	0.48	n/a	1.72	0.261	0.184	0.365	0.190	0.033	0.065	0.122	0.046	0.235	0.034	0.046	0.119	0.034	0.168	0.033	0.065
HKY	25	5092.360	4898.538	-2424.231	n/a	n/a	1.71	0.261	0.184	0.365	0.190	0.033	0.065	0.122	0.046	0.235	0.034	0.046	0.119	0.034	0.168	0.033	0.065
TN93+I	27	5094.779	4885.457	-2415.685	0.48	n/a	1.72	0.261	0.184	0.365	0.190	0.033	0.065	0.089	0.047	0.286	0.034	0.047	0.145	0.034	0.123	0.033	0.065
TN93	26	5099.911	4898.338	-2423.128	n/a	n/a	1.71	0.261	0.184	0.365	0.190	0.033	0.065	0.089	0.047	0.285	0.034	0.047	0.144	0.034	0.123	0.033	0.065
GTR+G+I	31	5103.576	4863.258	-2400.571	0.48	0.05	1.33	0.261	0.184	0.365	0.190	0.054	0.069	0.094	0.076	0.236	0.041	0.049	0.119	0.032	0.129	0.040	0.061
GTR+G	30	5104.012	4871.442	-2405.667	n/a	0.05	1.28	0.261	0.184	0.365	0.190	0.053	0.071	0.091	0.075	0.235	0.042	0.051	0.119	0.034	0.125	0.040	0.065
GTR+I	30	5124.023	4891.454	-2415.673	0.48	n/a	1.23	0.261	0.184	0.365	0.190	0.052	0.073	0.089	0.074	0.232	0.042	0.052	0.117	0.036	0.123	0.041	0.069
GTR	29	5129.257	4904.437	-2423.168	n/a	n/a	1.23	0.261	0.184	0.365	0.190	0.052	0.073	0.089	0.074	0.232	0.042	0.053	0.117	0.036	0.122	0.041	0.070
T92+G+I	25	5157.658	4963.836	-2456.880	0.48	0.05	1.80	0.223	0.223	0.277	0.277	0.039	0.049	0.179	0.039	0.179	0.049	0.039	0.144	0.049	0.144	0.039	0.049
T92+G	24	5157.765	4971.693	-2461.812	n/a	0.05	1.75	0.223	0.223	0.277	0.277	0.040	0.050	0.177	0.040	0.177	0.050	0.040	0.142	0.050	0.142	0.040	0.050
K2+G	23	5164.394	4986.072	-2470.004	n/a	0.05	1.74	0.250	0.250	0.250	0.250	0.046	0.046	0.159	0.046	0.159	0.046	0.046	0.159	0.046	0.159	0.046	0.046
K2+G+I	24	5164.439	4978.366	-2465.148	0.48	0.05	1.79	0.250	0.250	0.250	0.250	0.045	0.045	0.160	0.045	0.160	0.045	0.045	0.160	0.045	0.160	0.045	0.045
T92+I	24	5177.338	4991.265	-2471.598	0.48	n/a	1.71	0.223	0.223	0.277	0.277	0.041	0.051	0.176	0.041	0.176	0.051	0.041	0.141	0.051	0.141	0.041	0.051
JC+G	22	5177.412	5006.840	-2481.391	n/a	0.05	0.50	0.250	0.250	0.250	0.250	0.083	0.083	0.083	0.083	0.083	0.083	0.083	0.083	0.083	0.083	0.083	0.083
JC+G+I	23	5177.765	4999.443	-2476.689	0.48	0.05	0.50	0.250	0.250	0.250	0.250	0.083	0.083	0.083	0.083	0.083	0.083	0.083	0.083	0.083	0.083	0.083	0.083
T92	23	5182.430	5004.108	-2479.022	n/a	n/a	1.71	0.223	0.223	0.277	0.277	0.041	0.051	0.176	0.041	0.176	0.051	0.041	0.141	0.051	0.141	0.041	0.051
K2+I	23	5183.687	5005.365	-2479.651	0.48	n/a	1.71	0.250	0.250	0.250	0.250	0.046	0.046	0.158	0.046	0.158	0.046	0.046	0.158	0.046	0.158	0.046	0.046
K2	22	5188.922	5018.351	-2487.146	n/a	n/a	1.70	0.250	0.250	0.250	0.250	0.046	0.046	0.158	0.046	0.158	0.046	0.046	0.158	0.046	0.158	0.046	0.046
JC+I	22	5196.551	5025.979	-2490.960	0.48	n/a	0.50	0.250	0.250	0.250	0.250	0.083	0.083	0.083	0.083	0.083	0.083	0.083	0.083	0.083	0.083	0.083	0.083
JC	21	5201.785	5038.964	-2498.455	n/a	n/a	0.50	0.250	0.250	0.250	0.250	0.083	0.083	0.083	0.083	0.083	0.083	0.083	0.083	0.083	0.083	0.083	0.083

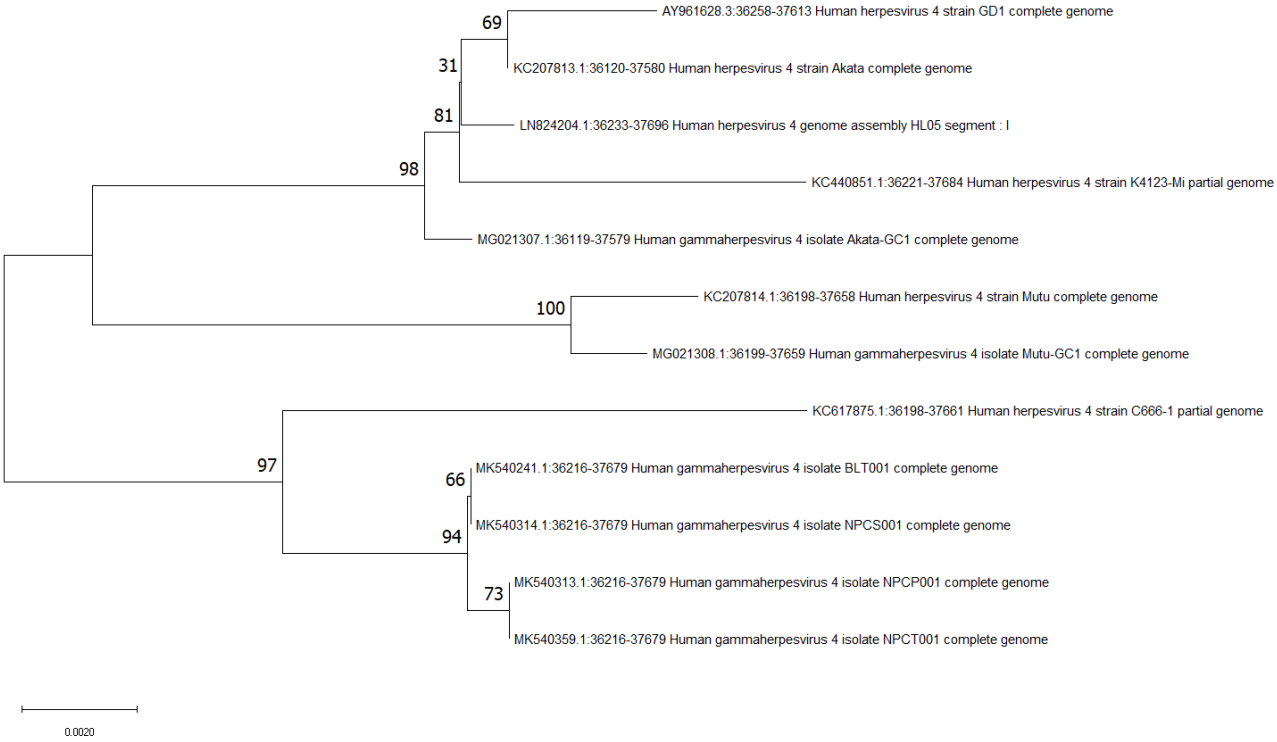

Figure 1: Maximum likelihood phylogenetic tree constructed by using bootstrap data.

Deletions

The nucleotide sites deleted for each sample when compared with reference gene KC617875 are listed in the first column. The accession number of samples that have the corresponding mutation is listed in the second column.

In the third column, the amino acid change or deletion caused by the nucleotide deletion mutation is listed.

Insertions

The nucleotide sites inserted for each sample when compared with reference gene KC617875 are listed in the first column.

The accession number of samples that have the corresponding mutation is listed in the second column. In the third column, the amino acid insertion that is caused by the nucleotide insertion mutation is listed.

Unknown mutation

The nucleotide sites that have unknown mutations for each sample when compared with reference gene KC617875 are listed in the first column. The accession number of samples that have the corresponding mutation is listed in the second column.

In the third column, the amino acid change or deletion that is caused by the nucleotide deletion mutation is listed.

Substitution Model Analysis and Phylogenetic Tree Construction

Nucleotide substitution models were analysed by using sample nucleotide sequences. The analysis is done by using an automatically created neighbour joining tree with the maximum likelihood method and all the nucleotide sites were used. The model analysed are combinations of 5 substitution models General Time Reversible (GTR), Hasegawa-Kishino-Yano (HKY), Tamura-Nei (TN93), Tamura 3-parameter (T92), Kimura 2-parameter (K2) or Jukes-Cantor (JC) with 3 rates among sites, gamma distributed (G), has invariant sites (I) or gamma distributed with invariant sites (G+I) (Makarova et al., 2012). Bayesian Information Criterion (BIC) scores and Akaike Information Criterion corrected (AICc) values are arranged from lowest to highest. While log-likelihood values (InL) are arranged from highest to lowest (Banos, 2010). The model is arranged from the most desirable to undesirable.

The BIC value, AICc values and lnL value are the 3 criterion that are used to determine the desirability of the model, in which a lower BIC and AICc value correlates to a better fit (Vrieze, 2012). Out of 24 types of different nucleotide substitution models listed (table 3), Hasegawa-Kishino-Yano with gamma-distributed and invariant sites, the HKY+G+I model is the best model to be used as the BIC value and AICc values are the lowest among all model listed. In addition, the model has high InL value.

Maximum likelihood phylogenetic trees constructed by using normal and bootstrap data. The tree branched into 2 main clades with a branch length scale of 0.002 from a common ancestor where one clade is closely related to reference sample KC617875, this clade includes MK540241, MK540314, MK540313 and MK540359. Another clade is distantly related to KC617875, which includes AY961628, KC207813, LN824204, KC440851, MG021307, KC207814 and MG021308. Sample from closely related clades are mostly isolated from NPC sample in China except for MK540241 isolated from Burkitt Lymphoma sample in China. In distantly related clades, most of the samples are isolated from gastric cancer, Burkitt Lymphoma and Hodgkin Lymphoma except for AY961628 which were isolated form NPC. The bootstrap confidence values are shown on the node of each branch. Bootstrap value was set to 100 in which this indicates that the phylogenetic tree is constructed 100 times using the HKY+G+I model. Based on the generated trees, a particular branch occurring 100 times indicates high confidence rate, where this means that the occurrence of that particular branch is highly probable. The higher the value the more probable that the branch being real (Efron, Halloran, and Holmes 1996).

Phylogenetic constructed by using EBV EBNA-2 gene from 1 reference sample and 11 samples by using the maximum likelihood method and Hasegawa-Kishino-Yano with gamma-distributed and invariant sites, the HKY+G+I model is selected. All samples are branched according to their divergence and the bootstrap value of each branch is shown to indicate the desirability of the branch. It could be observed that the first major clade has a bootstrap value of more than 90 corresponding to occurrence rate of > 0.9. This indicates that high probability of the first major clade indicating diverging lineage between samples resulting in two major clades. Interesting observation to be made here is that the EBNA2 sequence from KC617875 and AY961628 are distally related even though the EBV sequence are from the same disease (NPC). Moreover, the MK540241 EBNA2 sequence share similar lineage between most of the EBV in NPC, indicating high similarity between the EBNA2 sequence in Burkitt's lymphoma (BL) and NPC. Bootstrap value of 100 of the second major clade (from top) indicates total occurrence. This could also predict that EBNA2 sequence in KC207814 from BL and MG021308 from gastric cancer (GC) share a close similarity, it is interesting to note here also that geographical region also varies in these two samples, the BL sample was from Kenya while GC sample was from Poland. The gastric cancer sample isolated from the United Kingdom is the most diverged with 5 unique mutation sites identified.

4 types of known mutation and 1 unknown mutation have been identified from multiple sequence alignments performed by comparing 11 samples with reference sample KC617875. Out of 4 types of known mutation, which are missense, silent, deletion and insertion, missense mutation was most frequently identified, which causes change in encoded amino acids. However, the effect of these amino acid changes is not well known. For insertion

mutation, which is of the lowest frequency, was identified only once in KC207814 and MG021307 respectively, where insertion of nucleotide CTC has been identified in-between nucleotide sequence 633 to 637 and caused insertion of amino acid leucine at position 212. EBNA-2 gene of the C666-1 cell line was used as a reference as C666-1 consistently maintains EBV in long-term culture, providing an excellent in vitro model for EBV EBNA-2 comparative study (Cheung et al., 1999). The use of the EBNA-2 gene from the C666-1 cell line enables the comparison of variation of the EBNA-2 gene in NPC samples with the EBNA-2 gene of other diseases which are Burkitt Lymphoma, gastric cancer, and Hodgkin Lymphoma.

The nucleotide deletion identified in NPC sample (AY961628), Burkitt Lymphoma (KC207813, KC20814) and gastric cancer (MG021307, MG021308) which is the deletion of amino acid from position 63 to 95, and amino acids change at 62, 66, 67 and 68 have a similar scenario with previous research of Harada et al. (2001) where the deletion occur from position 59 to 95. Deletion within this range did not affect the self-association of EBNA-2 in vitro or in vivo but inhibited the ability to maintain higher-order structures in non-denaturing gels (Harada et al., 2001). Since EBNA2 acts as viral transcription factor, the stability of protein structures are crucial for transcription factor (TF) functioning as disruption in the structure could impair DNA binding capacity which could lead to a lower efficiency in TF functioning (Wu et al., 1996; Krieger et al., 2022).

Next, the deletions identified in AY961628, KC207813, KC207814, MG021307 and MG021308 from amino acids ranging from position 63 to 95 were also reported previously. Yalamanchili and group reported that the deletion of amino acids from position 2 to 88 resulted in minor effects on primary B lymphocyte transformation efficiency (Yalamanchili et al., 1996). In addition, the deletion of amino acids from position 358 to 359 were also validated experimentally where amino acids from position 333 to 425 were identified to be deleted and this resulted in the impairment of lymphocyte transformation (Cohen et al., 1991). Besides, the deletion of amino acids from position 358 to 359 was also suggested to influence the RG domain of the EBNA-2 gene (Wang et al., 2012). As mentioned earlier, the changes in amino acid sequence could affect crucial structure EBNA2 (Wu et al. 1996; Krieger et al. 2022). This could lead to lower activity which could result in impairment of lymphocyte transformation, or these changes would result in insignificant changes thus not affecting EBNA2 crucial function. Further research is needed to truly elucidate the actual mechanism.

Conclusion

The divergence of the ENBA-2 gene increases concerning geographical regions when compared to the EBNA2 sequence of EBV in C666-1 NPC. Three major clades indicate high variation of the EBNA2 sequence across disease samples. Although differences were observed, some sequences showed close lineage especially with EBNA2 from BL, this includes sequence from GC and NPC, despite originating from different diseases. Thus, is it worth to further investigate on the mechanistic events that could arise from these variations which could help in further advancing the knowledge of EBV contribution towards disease development.

Author Contributions

L.W.Z., R.B.S.M.N.M conceptualized and designed the study. L.W.Z., A.A., M.Y.M collected and analyzed the data, drafted the manuscript. All authors critically reviewed and approved the final version.

Acknowledgment

The authors acknowledged the Ministry of Higher Education, Malaysia for supporting this work through the Fundamental Research Grant Scheme Project Code (FRGS/1/2021/SKK03/USM/02/3) and for the facilities provided by the Universiti Sains Malaysia.

Competing financial interests

The authors have no conflict of interest.

References

Cabanas, H., Harnois, T., Magaud, C., Cousin, L., Constantin, B., Bourmeyster, N., & Déliot, N. (2018). Deregulation of calcium homeostasis in Bcr-Abl-dependent chronic myeloid leukemia. Oncotarget, 9(41), 26309–26327. https://doi.org/10.18632/oncotarget.25241

Cheng, H., Wang, S., & Feng, R. (2016). STIM1 plays an important role in TGF-β-induced suppression of breast cancer cell proliferation. Oncotarget, 7(13), 16866–16878. https://doi.org/10.18632/oncotarget.7619

Cheng, Y., Hao, Y., Zhang, A., Hu, C., Jiang, X., Wu, Q., & Xu, X. (2018). Persistent STAT5-mediated ROS production and involvement of aberrant p53 apoptotic signaling in the resistance of chronic myeloid leukemia to imatinib. International Journal of Molecular Medicine, 41(1), 455–463. https://doi.org/10.3892/ijmm.2017.3205

Cui, C., Merritt, R., Fu, L., & Pan, Z. (2017). Targeting calcium signaling in cancer therapy. Acta Pharmaceutica Sinica. B, 7(1), 3–17. https://doi.org/10.1016/j.apsb.2016.11.001

Dejos, C., Gkika, D., & Cantelmo, A. R. (2020). The Two-Way Relationship Between Calcium and Metabolism in Cancer. Frontiers in Cell and Developmental Biology, 8, 573747. https://doi.org/10.3389/fcell.2020.573747

Diez-Bello, R., Jardin, I., Salido, G. M., & Rosado, J. A. (2017). Orai1 and Orai2 mediate store-operated calcium entry that regulates HL60 cell migration and FAK phosphorylation. Biochimica Et Biophysica Acta. Molecular Cell Research, 1864(6), 1064–1070. https://doi.org/10.1016/j.bbamcr.2016.11.014

Feldman, B., Fedida-Metula, S., Nita, J., Sekler, I., & Fishman, D. (2010). Coupling of mitochondria to store-operated Ca(2+)-signaling sustains constitutive activation of protein kinase B/Akt and augments survival of malignant melanoma cells. Cell Calcium, 47(6), 525–537. https://doi.org/10.1016/j.ceca.2010.05.002

Feno, S., Butera, G., Vecellio Reane, D., Rizzuto, R., & Raffaello, A. (2019). Crosstalk between Calcium and ROS in Pathophysiological Conditions. Oxidative Medicine and Cellular Longevity, 2019, 9324018. https://doi.org/10.1155/2019/9324018

Ge, C., Zeng, B., Li, R., Li, Z., Fu, Q., Wang, W., Wang, Z., Dong, S., Lai, Z., Wang, Y., Xue, Y., Guo, J., Di, T., & Song, X. (2019). Knockdown of STIM1 expression inhibits non-small-cell lung cancer cell proliferation in vitro and in nude mouse xenografts. Bioengineered, 10(1), 425–436. https://doi.org/10.1080/21655979.2019.1669518

Görlach, A., Bertram, K., Hudecova, S., & Krizanova, O. (2015). Calcium and ROS: A mutual interplay. Redox Biology, 6, 260–271. https://doi.org/10.1016/j.redox.2015.08.010

Gross, S., Mallu, P., Joshi, H., Schultz, B., Go, C., & Soboloff, J. (2020). Ca2+ as a therapeutic target in cancer. Advances in Cancer Research, 148, 233–317. https://doi.org/10.1016/bs.acr.2020.05.003

Hempel, N., & Trebak, M. (2017). Crosstalk between calcium and reactive oxygen species signaling in cancer. Cell Calcium, 63, 70–96. https://doi.org/10.1016/j.ceca.2017.01.007

Herbst, R. S., Morgensztern, D., & Boshoff, C. (2018). The biology and management of non-small cell lung cancer. Nature, 553(7689), 446–454.

Jardin, I., & Rosado, J. A. (2016). STIM and calcium channel complexes in cancer. Biochimica Et Biophysica Acta, 1863(6 Pt B), 1418–1426. https://doi.org/10.1016/j.bbamcr.2015.10.003

Kim, J.-H., Lkhagvadorj, S., Lee, M.-R., Hwang, K.-H., Chung, H. C., Jung, J. H., Cha, S.-K., & Eom, M. (2014). Orai1 and STIM1 are critical for cell migration and proliferation of clear cell renal cell carcinoma. Biochemical and Biophysical Research Communications, 448(1), 76–82. https://doi.org/10.1016/j.bbrc.2014.04.064

Kondratska, K., Kondratskyi, A., Yassine, M., Lemonnier, L., Lepage, G., Morabito, A., Skryma, R., & Prevarskaya, N. (2014). Orai1 and STIM1 mediate SOCE and contribute to apoptotic resistance of pancreatic adenocarcinoma. Biochimica Et Biophysica Acta, 1843(10), 2263–2269. https://doi.org/10.1016/j.bbamcr.2014.02.012

Latour, S., Mahouche, I., Cherrier, F., Merlio, J.-P., Poglio, S., & Bepoldin, L. B. (2017). Abstract 1881: STIM1 and Orai1 control non-Hodgkin lymphoma cells migration. Cancer Research, 77(13_Supplement), 1881. https://doi.org/10.1158/1538-7445.AM2017-1881

Li, G., Zhang, Z., Wang, R., Ma, W., Yang, Y., Wei, J., & Wei, Y. (2013). Suppression of STIM1 inhibits human glioblastoma cell proliferation and induces G0/G1 phase arrest. Journal of Experimental & Clinical Cancer Research : CR, 32(1), 20. https://doi.org/10.1186/1756-9966-32-20

Li, W., Zhang, M., Xu, L., Lin, D., Cai, S., & Zou, F. (2013). The apoptosis of non-small cell lung cancer induced by cisplatin through modulation of STIM1. Experimental and Toxicologic Pathology: Official Journal of the Gesellschaft Fur Toxikologische Pathologie, 65(7–8), 1073–1081. https://doi.org/10.1016/j.etp.2013.04.003

Li, X., Fang, P., Mai, J., Choi, E. T., Wang, H., & Yang, X. (2013). Targeting mitochondrial reactive oxygen species as novel therapy for inflammatory diseases and cancers. Journal of Hematology & Oncology, 6, 19. https://doi.org/10.1186/1756-8722-6-19

Liu, Y., Jin, M., Wang, Y., Zhu, J., Tan, R., Zhao, J., Ji, X., Jin, C., Jia, Y., Ren, T., & Xing, J. (2020). MCU-induced mitochondrial calcium uptake promotes mitochondrial biogenesis and colorectal cancer growth. Signal Transduction and Targeted Therapy, 5(1), 59. https://doi.org/10.1038/s41392-020-0155-5

Lunz, V., Romanin, C., & Frischauf, I. (2019). STIM1 activation of Orai1. Cell Calcium, 77, 29–38. https://doi.org/10.1016/j.ceca.2018.11.009

Muik, M., Schindl, R., Fahrner, M., & Romanin, C. (2012). Ca(2+) release-activated Ca(2+) (CRAC) current, structure, and function. Cellular and Molecular Life Sciences: CMLS, 69(24), 4163–4176. https://doi.org/10.1007/s00018-012-1072-8

Perillo, B., Di Donato, M., Pezone, A., Di Zazzo, E., Giovannelli, P., Galasso, G., Castoria, G., & Migliaccio, A. (2020). ROS in cancer therapy: The bright side of the moon. Experimental & Molecular Medicine, 52(2), 192–203. https://doi.org/10.1038/s12276-020-0384-2

Prakriya, M. (2020). Calcium and cell function. The Journal of Physiology, 598(9), 1647–1648. https://doi.org/10.1113/JP279541

Rosado, J. A., Diez, R., Smani, T., & Jardín, I. (2015). STIM and Orai1 Variants in Store-Operated Calcium Entry. Frontiers in Pharmacology, 6, 325. https://doi.org/10.3389/fphar.2015.00325

Saint Fleur-Lominy, S., Maus, M., Vaeth, M., Lange, I., Zee, I., Suh, D., Liu, C., Wu, X., Tikhonova, A., Aifantis, I., & Feske, S. (2018). STIM1 and STIM2 Mediate Cancer-Induced Inflammation in T Cell Acute Lymphoblastic Leukemia. Cell Reports, 24(11), 3045-3060.e5. https://doi.org/10.1016/j.celrep.2018.08.030

Singh, A. K., Roy, N. K., Bordoloi, D., Padmavathi, G., Banik, K., Khwairakpam, A. D., Kunnumakkara, A. B., & Sukumar, P. (2020). Orai-1 and Orai-2 regulate oral cancer cell migration and colonisation by suppressing Akt/mTOR/NF-κB signalling. Life Sciences, 261, 118372.

Takahashi, N., Chen, H.-Y., Harris, I. S., Stover, D. G., Selfors, L. M., Bronson, R. T., Deraedt, T., Cichowski, K., Welm, A. L., Mori, Y., Mills, G. B., & Brugge, J. S. (2018). Cancer Cells Co-opt the Neuronal Redox-Sensing Channel TRPA1 to Promote Oxidative-Stress Tolerance. Cancer Cell, 33(6), 985-1003.e7. https://doi.org/10.1016/j.ccell.2018.05.001

Tilly, H., Silva, M. G. da, Vitolo, U., Jack, A., Meignan, M., Lopez-Guillermo, A., Walewski, J., André, M., Johnson, P. W., Pfreundschuh, M., & Ladetto, M. (2015). Diffuse large B-cell lymphoma (DLBCL): ESMO Clinical Practice Guidelines for diagnosis, treatment and follow-up†. Annals of Oncology, 26, v116–v125. https://doi.org/10.1093/annonc/mdv304

Umemura, M., Baljinnyam, E., Feske, S., De Lorenzo, M. S., Xie, L.-H., Feng, X., Oda, K., Makino, A., Fujita, T., Yokoyama, U., Iwatsubo, M., Chen, S., Goydos, J. S., Ishikawa, Y., & Iwatsubo, K. (2014). Store-operated Ca2+ entry (SOCE)

regulates melanoma proliferation and cell migration. PloS One, 9(2), e89292. https://doi.org/10.1371/journal.pone.0089292

Vashisht, A., Trebak, M., & Motiani, R. K. (2015). STIM and Orai proteins as novel targets for cancer therapy. A Review in the Theme: Cell and Molecular Processes in Cancer Metastasis. American Journal of Physiology - Cell Physiology, 309(7), C457–C469. https://doi.org/10.1152/ajpcell.00064.2015

Wang, J., Zhang, C., Chen, K., Tang, H., Tang, J., Song, C., & Xie, X. (2015). ERβ1 inversely correlates with PTEN/PI3K/AKT pathway and predicts a favorable prognosis in triple-negative breast cancer. Breast Cancer Research and Treatment, 152(2), 255–269. https://doi.org/10.1007/s10549-015-3467-3

Wang, W., Ren, Y., Wang, L., Zhao, W., Dong, X., Pan, J., Gao, H., & Tian, Y. (2018). Orai1 and Stim1 Mediate the Majority of Store-Operated Calcium Entry in Multiple Myeloma and Have Strong Implications for Adverse Prognosis. Cellular Physiology and Biochemistry: International Journal of Experimental Cellular Physiology, Biochemistry, and Pharmacology, 48(6), 2273–2285. https://doi.org/10.1159/000492645

Yang, S., Zhang, J. J., & Huang, X.-Y. (2009). Orai1 and STIM1 Are Critical for Breast Tumor Cell Migration and Metastasis. Cancer Cell, 15(2), 124–134. https://doi.org/10.1016/j.ccr.2008.12.019

Zhao, H., Yan, G., Zheng, L., Zhou, Y., Sheng, H., Wu, L., Zhang, Q., Lei, J., Zhang, J., Xin, R., Jiang, L., Zhang, X., Chen, Y., Wang, J., Xu, Y., Li, D., & Li, Y. (2020). STIM1 is a metabolic checkpoint regulating the invasion and metastasis of hepatocellular carcinoma. Theranostics, 10(14), 6483–6499. https://doi.org/10.7150/thno.44025